

Cite this: *Chem. Sci.*, 2020, 11, 3845 All publication charges for this article have been paid for by the Royal Society of Chemistry



Received 5th February 2020

Accepted 16th March 2020

DOI: 10.1039/d0sc00690d

rsc.li/chemical-science

# Facilitating the reduction of V–O bonds on VO<sub>x</sub>/ZrO<sub>2</sub> catalysts for non-oxidative propane dehydrogenation†

Yufei Xie,  Ran Luo, Guodong Sun, Sai Chen, Zhi-Jian Zhao, Rentao Mu and Jinlong Gong \*

Supported vanadium oxide is a promising catalyst in propane dehydrogenation due to its competitive performance and low cost. Nevertheless, it remains a grand challenge to understand the structure–performance correlation due to the structural complexity of VO<sub>x</sub>-based catalysts in a reduced state. This paper describes the structure and catalytic properties of the VO<sub>x</sub>/ZrO<sub>2</sub> catalyst. When using ZrO<sub>2</sub> as the support, the catalyst shows six times higher turnover frequency (TOF) than using commercial γ-Al<sub>2</sub>O<sub>3</sub>. Combining H<sub>2</sub>-temperature programmed reduction, *in situ* Raman spectroscopy, X-ray photoelectron spectroscopy and theoretical studies, we find that the interaction between VO<sub>x</sub> and ZrO<sub>2</sub> can facilitate the reduction of V–O bonds, including V=O, V–O–V and V–O–Zr. The promoting effect could be attributed to the formation of low coordinated V species in VO<sub>x</sub>/ZrO<sub>2</sub> which is more active in C–H activation. Our work provides a new insight into understanding the structure–performance correlation in VO<sub>x</sub>-based catalysts for non-oxidative propane dehydrogenation.

## Introduction

Propylene is one of the most important chemical building blocks and its high-value derivatives are of great demand in the chemical industry. Due to the large-scale exploitation of shale gas, direct propane dehydrogenation becomes a particularly important method to produce propylene using propane as feedstock. Commercialized propane dehydrogenation plants generally utilize Pt-based and CrO<sub>x</sub>-based catalysts, however these two kinds of catalysts are either expensive or toxic.<sup>1</sup> Alternatively, supported vanadium oxide is a promising catalyst compared with Pt and CrO<sub>x</sub> for its competitive performance, low cost and low toxicity.<sup>2,3</sup>

It is well established that VO<sub>x</sub>-based catalysts can be utilized in propane oxidative dehydrogenation (ODH).<sup>4–8</sup> However, there is a trade-off effect between conversion and selectivity associated with over oxidation to CO<sub>x</sub>, which prevents the ODH process from achieving high propylene yield. In contrast, better reactivity and selectivity, especially excellent regeneration stability can be achieved when supported VO<sub>x</sub> catalysts are used in the non-oxidative propane dehydrogenation (PDH) process.<sup>9–13</sup> Nevertheless, the structure–performance

correlation of VO<sub>x</sub>-based catalysts is still unclear due to the structural complexity of the supported VO<sub>x</sub> catalytic system. Previous studies have confirmed that several factors could influence the performance of VO<sub>x</sub>-based catalysts such as polymerization forms of VO<sub>x</sub>, chemical states of V and the identity of the support.<sup>14–18</sup>

The support effect is an essential parameter because VO<sub>x</sub> can be bonded to a support through the V–O–support interaction. The variety of supports could lead to significant changes in the catalytic properties of VO<sub>x</sub>. It is generally accepted that the support could affect reactivity by stabilizing the active sites and/or altering the electron state of active sites.<sup>19–22</sup> The support effect has been extensively studied over VO<sub>x</sub>-based catalysts in the ODH process. Researchers have concluded that the lattice oxygen in V=O and V–O–support (V–O–S) bonds is consumed in C–H activation and H<sub>2</sub>O is formed. Thus, support identities could affect the reaction by tuning the oxygen vacancy formation energy, which is confirmed by experiments and DFT calculations.<sup>23–25</sup>

However, the support effect works in an entirely different way in the PDH process because not only active sites but also reaction mechanisms are distinct from those of the ODH process. V–O bonds directly catalyze C–H activation forming H<sub>2</sub> rather than H<sub>2</sub>O. Previous studies found that the reactivity of PDH is dependent on the bond strength of V–O–S.<sup>22</sup> It is proposed that V–O–S bonds are active sites. In addition, the support identity also influences the behavior of carbon deposition on VO<sub>x</sub> based catalysts, which inversely affects activity and on-stream stability.<sup>12,18</sup> Nevertheless, the effect of a support

Key Laboratory for Green Chemical Technology of Ministry of Education, School of Chemical Engineering and Technology, Tianjin University, Collaborative Innovation Center of Chemical Science and Engineering, Tianjin 300072, China. E-mail: jlgong@tju.edu.cn

† Electronic supplementary information (ESI) available. See DOI: 10.1039/d0sc00690d



is still not clear because the structure of  $\text{VO}_x$  and the  $\text{VO}_x$ -support interface in a reduced state is still ambiguous.

Herein, we explore the support effect on the catalytic performance of  $\text{VO}_x$ -based catalysts for PDH and provide a new insight into understanding how support identity matters. We discovered that  $\text{VO}_x/\text{ZrO}_2$ , a well-known catalyst for ODH,<sup>26–28</sup> has a much more superior PDH performance than commonly used  $\text{VO}_x/\text{Al}_2\text{O}_3$ . The turnover frequency (TOF) is six times higher by loading  $\text{VO}_x$  on  $\text{ZrO}_2$  than on  $\text{Al}_2\text{O}_3$ . The remarkable improvement of reactivity has not been reported in previous studies. Rate measurement of catalysts with gradient V loadings was employed to identify the active site of the  $\text{VO}_x/\text{ZrO}_2$  catalyst. *In situ* Raman spectroscopic measurements, X-ray photoelectron spectroscopy (XPS) and density functional theory (DFT) calculations were used to determine the structure evolution of  $\text{VO}_x$  under a reducing atmosphere, and they show that many more V–O bonds on  $\text{ZrO}_2$  (V=O, V–O–V and V–O–Zr) are consumed during reduction. On this basis, we proposed that the facile reducing nature of V–O bonds promotes the formation of lower coordinated V species which accounts for C–H activation enhancement.

## Results and discussion

### Catalyst structure

A series of characterization techniques were used to determine the bulk and surface structure of the catalysts ( $\text{VO}_x$  loaded on  $\text{ZrO}_2$  and  $\text{Al}_2\text{O}_3$  are denoted as  $x\text{VZr}$  and  $x\text{VAL}$  where  $x$  represents the mass percentage of V, metal base). The bare  $\text{ZrO}_2$  support, 1VZr and 1VAL were characterized by X-ray diffraction (XRD). As shown in Fig. 1a,  $\text{ZrO}_2$  is mainly composed of monoclinic phase (m- $\text{ZrO}_2$ , JCPDS 72-1669) with small amount of a tetragonal phase (t- $\text{ZrO}_2$ , JCPDS 79-1771), which is consistent with the previous report using the same preparation method.<sup>29</sup> The same XRD pattern of 1VZr and pure  $\text{ZrO}_2$  indicates that  $\text{VO}_x$  does not change the crystalline structure of  $\text{ZrO}_2$ . In addition, for  $\text{VO}_x$  loaded catalysts, only diffraction lines of the support could be detected (Fig. 1a and S1a†), which means amorphous  $\text{VO}_x$  is well dispersed on these catalysts.<sup>30,31</sup>

Vis-Raman spectroscopic measurements, which are sensitive to the presence of  $\text{V}_2\text{O}_5$ , were performed over the catalysts to gain insight into the kind of vanadium species. Raman spectra of the  $\text{ZrO}_2$  support, 1VZr and 1VAL are displayed in Fig. 1b. A band at  $1011\text{ cm}^{-1}$  is attributed to vanadyl stretching of surface-dispersed  $\text{VO}_x$ . No sharp band at  $995\text{ cm}^{-1}$ , assigned to the stretching vibration of V=O in crystal  $\text{V}_2\text{O}_5$ , is detected. With the V loading increasing, a band characteristic of  $\text{V}_2\text{O}_5$  at  $995\text{ cm}^{-1}$  appears after the loading reached 3 wt% (Fig. S1b†). This demonstrates the existence of crystal  $\text{V}_2\text{O}_5$  in 3VZr and 4VZr. From the enlarged region on the left from 75 to  $160\text{ cm}^{-1}$ , a small band which corresponds to  $\text{V}_2\text{O}_5$  at around  $150\text{ cm}^{-1}$  can be seen in 2.5VZr. This implies that  $\text{VO}_x$  begins to crystallize at 2.5VZr. Besides, the absence of a peak at around  $770\text{ cm}^{-1}$  suggests no  $\text{ZrV}_2\text{O}_7$  is formed in our samples.<sup>32</sup> The Raman spectra demonstrate that  $\text{VO}_x$  species are well dispersed as oligomeric species when the loading is less than 2 wt% and  $\text{V}_2\text{O}_5$  crystals are formed after the loading reaches 2.5 wt%.

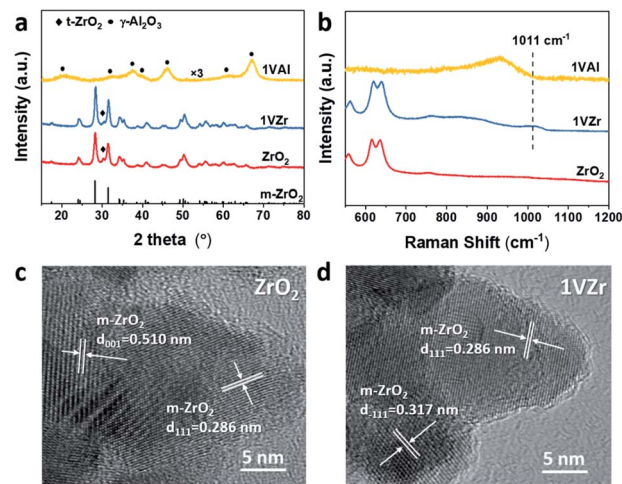


Fig. 1 (a) XRD patterns of the  $\text{ZrO}_2$  support and  $\text{VO}_x$  supported on  $\text{ZrO}_2$  and  $\text{Al}_2\text{O}_3$ . (b) Raman spectra (532 nm excitation) of the  $\text{ZrO}_2$  support and  $\text{VO}_x$  supported on  $\text{ZrO}_2$  and  $\text{Al}_2\text{O}_3$ . TEM images of (c)  $\text{ZrO}_2$  and (d)  $\text{VO}_x/\text{ZrO}_2$ .

Surface density of V was calculated through the BET surface area and V loading. The detailed results are listed in Table S1.† 2.5VZr has a V density of  $6.9\text{ nm}^{-2}$  which is a bit lower than the theoretical monolayer coverage. It has been proved that the presence of  $\text{V}_2\text{O}_5$  is inevitable below theoretical monolayer coverage by a simple incipient wetness impregnation method.<sup>10</sup> This agrees with the observation of the  $\text{V}_2\text{O}_5$  peak in 2.5VZr through Raman spectroscopic measurements.

The morphologies of  $\text{ZrO}_2$  and 1VZr were also characterized by TEM (Fig. 1c and d).  $\text{ZrO}_2$  is in the form of a nanoparticle with a relevant uniform size of around 30 nm and its morphology does not change after loaded with  $\text{VO}_x$ . Lattice

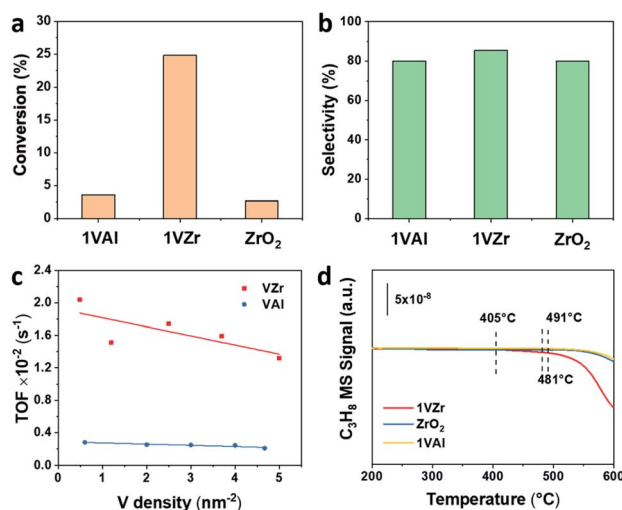


Fig. 2 (a) Initial propane conversion and (b) propylene selectivity (based on all products) of 1VAL, 1VZr and  $\text{ZrO}_2$ . Reaction conditions:  $m_{\text{cat}} = 0.4\text{ g}$ ;  $\text{C}_3\text{H}_8 : \text{N}_2 : \text{H}_2 = 7 : 36 : 7$ ;  $T = 550\text{ }^\circ\text{C}$ ; inlet flow =  $50\text{ mL min}^{-1}$ . (c) Comparison of TOF values between VZr and VAL with different V densities. (d)  $\text{C}_3\text{H}_8$ -TPSR of 1VZr,  $\text{ZrO}_2$  and 1VAL.



fringes of  $V_2O_5$  could not be found because amorphous  $VO_x$  is well dispersed on the surface of  $ZrO_2$ . The TEM results are in good agreement with the observations of XRD and Raman results.

### Catalytic performance

Catalytic performance of  $VO_x$  supported on  $ZrO_2$  and  $\gamma-Al_2O_3$  for the PDH reaction was studied. The initial propane conversion and propylene selectivity based on all products are illustrated in Fig. 2a and b. The initial conversion of 1VZr is approximately five times higher than that of 1VAL and pure  $ZrO_2$ , which shows a significant support effect. The total selectivity towards propylene is around 80% and gas-phase selectivity towards it is >90% (Fig. S2a†) for all catalysts, which are at a similar level with respect to those of the  $VO_x$ -based catalysts in previous studies.<sup>10,14,18,33</sup> In addition, we performed 120 min of the on stream reaction and studied the reaction–regeneration cycles over 1VZr (Fig. S2b and S3†). The propane conversion and propylene selectivity exhibit little change during six cycles, implying outstanding regeneration stability.

Because the surface areas of  $ZrO_2$  and  $Al_2O_3$  are different, when the V loadings of VZr and VAL are identical, they have different V densities. Considering the activity is also influenced by V density, the TOFs of VZr and VAL were also compared based on V density (Fig. 2c and Table S2†). The calculated TOF of VZr is almost 6-fold higher than that of VAL and only slightly decreases with the V surface density, which implies that the activity is strongly support-dependent. This phenomenon is similar to that of the  $GaO_x$  catalytic system, where the activity is not a consequence of Ga nuclearities, but of the Ga–O–support interaction.<sup>34</sup>

To further evaluate the intrinsic activity in C–H activation, propane temperature-programmed surface reaction ( $C_3H_8$ -TPSR) experiments were carried out over 1VZr,  $ZrO_2$  and 1VAL. The temperature where the  $C_3H_8$  signal begins to drop is determined as the C–H activation temperature. As shown in Fig. 2d, the initial C–H activation temperature of 1VZr is around 405 °C, which is almost 80 and 90 °C lower than that of  $ZrO_2$  (481 °C) and 1VAL (491 °C). Moreover, the C–H activation temperature of 3VAL (similar V density to 1VZr, Fig. S4†) was also tested, which is 100 °C higher than that of 1VZr. Along with the TOF difference between VZr and VAL, we can conclude that the intrinsic C–H activation ability of 1VZr is distinguishable.

### Active phase identification

It has been proved that pure  $ZrO_2$  can also catalyze propane dehydrogenation through coordinatively unsaturated Zr ( $Zr_{cus}$ ).<sup>35–37</sup> In addition, Jeon *et al.* prepared V–Zr mix oxide and found that V incorporation into the  $ZrO_2$  bulk phase would promote generation of more  $Zr_{cus}$ .<sup>38</sup> Although in our  $VO_x/ZrO_2$  system,  $VO_x$  is supported on the surface of a support, not in the bulk phase, there still remains different possibilities for this superior performance of the  $VO_x/ZrO_2$  catalyst:  $ZrO_2$  enhances the activity of  $VO_x$ ,  $VO_x$  enhances the activity of  $ZrO_2$  ( $Zr_{cus}$ ), or a combination of the two. Therefore, it is essential to verify if the active phase is  $VO_x$  or  $Zr_{cus}$  in order to understand the origin of

this dramatic performance improvement. To this end, various experiments were performed to figure out whether the catalytic performance is due to  $VO_x$  or  $Zr_{cus}$  or both of them.

The propane consumption rate *versus* V loading is shown in Fig. 3. The reaction rate rises linearly as the V loading increases until the V loading reaches 2 wt%, indicating  $VO_x$  should be the active component. After this linearly increasing period, the  $C_3H_8$  consumption rate does not change with increasing V loading because full  $VO_x$  overlayers are formed at 2 wt% and crystallized  $V_2O_5$  appears afterward as confirmed by the Raman spectra (Fig. S1b†). In addition, previous articles reported a shift of XPS Zr 3d peaks and reduction peaks of  $ZrO_2$  seen in the  $H_2$  temperature programmed reduction ( $H_2$ -TPR) profile if  $Zr_{cus}$  is the active site.<sup>37,39,40</sup> However, these phenomena cannot be observed in the  $VO_x/ZrO_2$  system. No  $ZrO_2$  reduction peak can be observed up to 600 °C (Fig. 4a), while our reactions were conducted at 550 °C. In addition, the XPS test also confirms that the binding energy of Zr 3d in  $ZrO_2$  and 1VZr has no difference (Fig. S5†). These results provide evidence that  $ZrO_2$  is not the



Fig. 3  $C_3H_8$  reaction rate *versus* different V loadings on VZr catalysts at 550 °C.



Fig. 4 (a)  $H_2$ -TPR profiles of 1VZr, 1VAL and pure  $ZrO_2$ . (b) XPS O 1s and V 2p peaks for 1VZr and 1VAL. Deconvolution results of V 2p<sub>3/2</sub> for (c) 1VZr and (d) 1VAL after reduction for 30 minutes.





active phase in VZr catalysts. Along with catalytic activity being linearly related to the amount of V, which directly proves  $\text{VO}_x$  is responsible for the activity, we suggest  $\text{VO}_x$  rather than  $\text{Zr}_{\text{cus}}$  to be the main active phase. However, it is a pity that these experiments cannot identify which kind of V–O bond (V=O, V–O–V, V–O–Zr or all of them) is responsible for C–H activation. A potential method to solve this problem is Surface Organometallic Chemistry (SOMC),<sup>41–43</sup> which provides access to producing well-defined isolated  $\text{VO}_x$  only possessing V=O and V–O–support. This direction still needs further investigation.

### Structure–performance correlation

$\text{H}_2$ -TPR experiments were performed to test the reducibility and  $\text{VO}_x$ –support interaction of the catalysts (Fig. 4a). The main peak at around 400–500 °C is attributed to the reduction of  $\text{VO}_x$  and peaks above 600 °C are ascribed to a partial reduction of  $\text{ZrO}_2$ .<sup>36,44–46</sup> The reduction temperature of  $\text{VO}_x$  for 1VZr is lower than that for 1VAL. Considering that the reduction temperature is influenced by the dispersion of  $\text{VO}_x$ ,<sup>15,47</sup> we performed  $\text{H}_2$ -TPR on a series of VAL and VZr catalysts (Fig. S6†). The reduction temperatures of VZr catalysts are at about 400 °C while those of VAL catalysts are at about 500 °C. Thus, the low reduction temperature of the VZr catalyst implies that the interaction between  $\text{VO}_x$  and  $\text{ZrO}_2$  is weaker than that between  $\text{VO}_x$  and  $\text{Al}_2\text{O}_3$ . This phenomenon is further discussed in the *in situ* Raman spectroscopy section below. Alternatively, the peak area of 1VZr is larger than that of 1VAL. We calculated the H : V ratio through the peak area and estimated the average oxidation state (AOS) of V. As listed in Table S3,† the AOS of V in 1VZr and 1VAL corresponds to 3.5 and 4.0, which indicates that  $\text{VO}_x$  can be more readily and deeply reduced on  $\text{ZrO}_2$ .

To further identify the valance state of V, XPS investigation was carried out over 1VZr and 1VAL after  $\text{H}_2$  reduction for 30 min. V 2p core levels of 1VZr and 1VAL are displayed in Fig. 4b. We compare the binding energy of V in different catalysts qualitatively. The binding energy of V 2p<sub>2/3</sub> centers at 516.5 eV in 1VZr and 517.5 eV in 1VAL. This indicates that the valance state of V in 1VZr is lower than that in 1VAL. According to the deconvolution results of V 2p shown in Fig. 4c, d and Table S4,† the oxidation state of V is a mixture of  $\text{V}^{5+}$ ,  $\text{V}^{4+}$  and  $\text{V}^{3+}$ , which is consistent with previous results.<sup>33,44,48</sup> The fraction of  $\text{V}^{3+}$  is 48.6% in 1VZr, which is higher than 6.6% in 1VAL.

It has been elucidated in the former articles that  $\text{V}^{3+}$  is more active in the PDH reaction.<sup>14,33</sup> However, seldom detailed analyzes have been conducted to identify the structure of  $\text{VO}_x$  in a reduced state and the structure–performance correlation is not clear. Therefore, *in situ* UV-Raman spectroscopy, which is more sensitive to the surface  $\text{VO}_x$  structure,<sup>49</sup> was performed to monitor the evolution of V=O, V–O–V, and the V–O–support.

The evolution of V–O–V, V–O–Zr and V=O in 1VZr during  $\text{H}_2$  reduction is shown in Fig. 5a and b. A broad band at 750–950  $\text{cm}^{-1}$  is ascribed to V–O–V and V–O–Zr bonds.<sup>32,50</sup> The band at around 1020  $\text{cm}^{-1}$  is assigned to V=O in dispersed  $\text{VO}_x$ .<sup>27,32,51</sup> The number of V–O–V and V–O–Zr bonds decreases substantially which implies that plenty of these bonds are consumed during reduction. In addition, nearly 60% of V=O in 1VZr disappeared after reduction

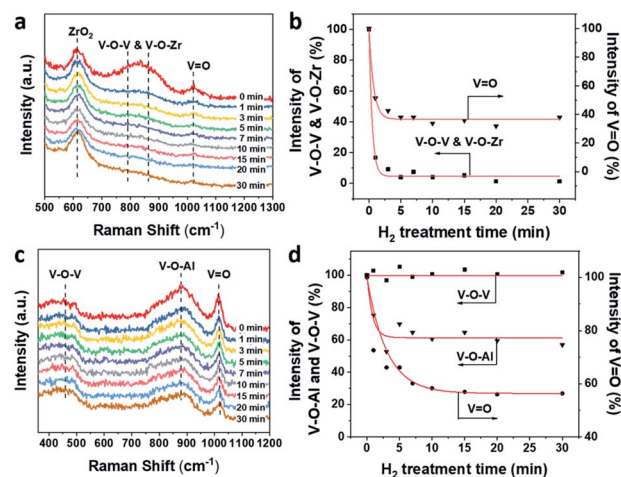


Fig. 5 (a) *In situ* UV-Raman (325 nm excitation) spectra of VZr during  $\text{H}_2$  reduction at 550 °C. (b) Intensities of V–O–V, V–O–Zr, and V=O versus  $\text{H}_2$  treatment time. (c) *In situ* UV-Raman (325 nm excitation) spectra of 1VAL during  $\text{H}_2$  reduction at 550 °C. (d) Intensities of V–O–V, V–O–Al and V=O versus  $\text{H}_2$  treatment time.

for 30 min. The comparative experiment of 1VAL is displayed in Fig. 5c and d. The bands attributed to V–O–V and V–O–Al on the  $\text{Al}_2\text{O}_3$  support are located at 400–600  $\text{cm}^{-1}$  and 910  $\text{cm}^{-1}$  respectively.<sup>49</sup> A sharp band at 1018  $\text{cm}^{-1}$  is ascribed to V=O.<sup>49</sup> In contrast with V–O–Zr and V–O–V in the 1VZr sample, the V–O–Al band only decreases to 60% of that for fresh 1VZr and no change of the V–O–V band is detected which implies V–O–V bonds on the  $\text{Al}_2\text{O}_3$  support cannot be reduced under  $\text{H}_2$  treatment. Meanwhile, 40% of V=O in 1VAL is reduced, which is less than that in 1VZr. The result of *in situ* Raman spectroscopy confirms that not only V=O and V–O–Zr, but also V–O–V can be deeply reduced in 1VZr which results in the deeper reduction degree of 1VZr observed in  $\text{H}_2$ -TPR and XPS studies.

The facile reduction nature of V–O bonds in the VZr catalyst can be interpreted by the lower electronegativity of Zr compared with Al, which causes the difference of the interaction between  $\text{VO}_x$  and the support. It has been shown that a lower support cation electronegativity can result in a higher electron density of the V–O–S bond, which lead to these bonds being readily reduced.<sup>52,53</sup> Along with the lower reduction temperature of VZr shown in the  $\text{H}_2$ -TPR profile, it can be deduced that the interaction between  $\text{VO}_x$  and  $\text{ZrO}_2$  weakens the V–O bonds thus resulting in the facile reduction nature of the VZr catalyst.

Note that when O atoms are removed during the reduction period, the chemical environment of V changes, which leads to the formation of coordinatively unsaturated V. It is established that metal cations ( $\text{Ga}^{3+}$ ,  $\text{Zn}^{2+}$ ,  $\text{Zr}^{4+}$ , etc.) with a low coordination number are more active for the reaction.<sup>54</sup> As more V–O bonds are reduced in the VZr catalyst, we could deduce that lower coordinated V sites are more active for the C–H activation. Our recent DFT calculations also proved that coordinatively unsaturated  $\text{VO}_x$  was more active in C–H activation<sup>55</sup> while this work gives experimental evidence.



**Table 1** Oxygen vacancy formation energies of vanadium supported on  $m\text{-ZrO}_2(111)$  and  $\gamma\text{-Al}_2\text{O}_3(100)$

|  | Oxygen vacancy formation energies (eV) |       |             |      |       |
|--|--|-------|-------------|------|-------|
|  | V=O                                    | V-O-V | V-O-support |      |       |
| $\text{V}_2\text{O}_5/m\text{-ZrO}_2(111)$               | 0.13                                   | -0.13 | 0.03        | 0.14 | 0.34  |
| $\text{V}_2\text{O}_5/\gamma\text{-Al}_2\text{O}_3(100)$ | -0.07                                  | 0.44  | 0.36        | 0.35 | -0.25 |

## DFT calculations

DFT calculations were conducted to gain further insight into the structure of the active site and its influence on catalytic performance. Noting that the TOF difference between VZr and VAl exists with all the V densities, we constructed dimeric vanadium oxide species on the  $m\text{-ZrO}_2(111)$  and  $\gamma\text{-Al}_2\text{O}_3(100)$  surface as representatives<sup>36,55</sup> (Fig. S7†).

We calculated oxygen vacancy formation energy of different oxygen atoms, with the energy of  $\text{H}_2\text{O}(\text{g})$  and  $\text{H}_2(\text{g})$  as the reference, in these vanadium oxide dimers to confirm the different reducibilities they showed in our experiment results. As listed in Table 1, oxygen atoms are removed from V=O, V-O-V and the V-O-support. Four of five V-O bonds in VZr (V=O, V-O-V and two V-O-Zr) have relatively low oxygen formation energies while only two of five in VAl do (V=O, V-O-Al). The calculated oxygen vacancy formation energies are in good agreement with the Raman spectroscopy result that V=O, V-O-V and V-O-Zr bonds in VZr can be reduced under a  $\text{H}_2$  atmosphere while only V=O and part of V-O-Al are reduced in VAl.

Since VZr and VAl have different degrees of reduction, we constructed  $\text{V}_2\text{O}_2/m\text{-ZrO}_2(111)$  and  $\text{V}_2\text{O}_3/\gamma\text{-Al}_2\text{O}_3(100)$  models to represent the catalyst structure in a reduced state (Fig. 6a and b). In terms of the *in situ* Raman results and calculated oxygen vacancy formation energies, three (one in each V=O, V-O-Zr and V-O-V) and two (one V=O and one V-O-Al) V-O bonds with the lowest oxygen vacancy formation energies were removed from the initial dimeric  $\text{V}_2\text{O}_5$  structure respectively. The propane dehydrogenation barriers over partially reduced VZr and VAl were computed and transition state (TS) geometries are shown in Fig. 6c. The first and second step C-H activation



**Scheme 1** Propane dehydrogenation on VZr and VAl catalysts with different V structures and  $\text{VO}_x$  reduction degrees.

barriers in VZr is 0.66 eV and 0.85 eV, respectively, while in VAl they are 0.99 eV and 1.26 eV, respectively. DFT calculations also confirm that low coordinated V species are more active in C-H activation, which is consistent with the highest TOF and the lowest C-H activation temperature for VZr observed in the catalytic performance and  $\text{C}_3\text{H}_8\text{-TPSR}$  tests.

Based on the experimental and theoretical results, we propose a structure-performance correlation of VZr and VAl catalysts, as shown in Scheme 1.  $\text{VO}_x$  can be readily reduced on  $\text{ZrO}_2$  because the interaction between  $\text{VO}_x$  and  $\text{ZrO}_2$  facilitates the reduction of V=O, V-O-V and V-O-Zr bonds. However, for the VAl catalyst, only V=O and some V-O-Al bonds can be reduced. Thus, more low coordinated V species form in the VZr catalyst during reduction, and these low coordinated V species exhibit a better performance in PDH.

## Conclusions

In summary, we prepared  $\text{VO}_x$  loaded on  $\text{ZrO}_2$  through a simple incipient wetness impregnation method, which exhibits a dramatically improved performance compared with  $\text{VO}_x$  loaded on  $\text{Al}_2\text{O}_3$  for propane dehydrogenation. The  $\text{TOF}_{\text{C}_3\text{H}_8}$  of 1VZr is determined to be  $0.0161 \text{ s}^{-1}$ , which is almost six times higher than that of 1VAl.

We further prove that the remarkable reactivity of the 1VZr catalyst was attributed to the promotion of C-H activation over  $\text{VO}_x$  species rather than it over  $\text{ZrO}_2$ . Besides, combining *in situ* Raman and XPS spectroscopy results, we propose the enhanced C-H activation on VZr results from the facile reduction of V=O, V-O-V and V-O-Zr bonds, thus producing deeply reduced and lower coordinated V species. DFT calculations also confirm that the C-H rupture energy barrier is lower for partially reduced VZr with low coordinated V species. Considering the dramatic performance achieved through the interaction between  $\text{VO}_x$  and  $\text{ZrO}_2$ , our work provides a new insight into high-performance  $\text{VO}_x$ -based catalysts for propane dehydrogenation.

## Conflicts of interest

There are no conflicts to declare.

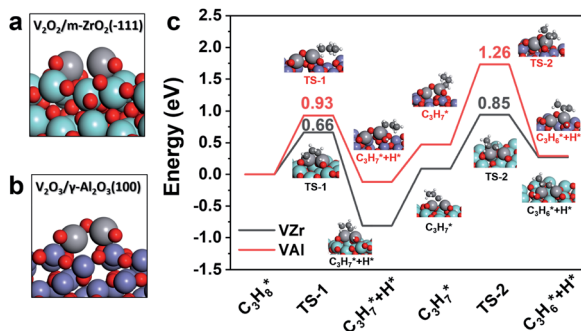


**Fig. 6** Reduced catalyst models of (a)  $\text{V}_2\text{O}_2/m\text{-ZrO}_2(111)$  and (b)  $\text{V}_2\text{O}_3/\gamma\text{-Al}_2\text{O}_3(100)$ . (c) Calculated potential energy diagrams of the first and second propane dehydrogenation step.



## Acknowledgements

We acknowledge the National Natural Science Foundation of China (21525626, and 51761145012), and the Program of Introducing Talents of Discipline to Universities (B06006) for financial support.

## Notes and references

- J. J. Sattler, J. Ruiz-Martinez, E. Santillan-Jimenez and B. M. Weckhuysen, *Chem. Rev.*, 2014, **114**, 10613–10653.
- S. Sokolov, M. Stoyanova, U. Rodemerck, D. Linke and E. V. Kondratenko, *J. Catal.*, 2012, **293**, 67–75.
- B. M. Weckhuysen and D. E. Keller, *Catal. Today*, 2003, **78**, 25–46.
- S. Barman, N. Maity, K. Bhatte, S. Ould-Chikh, O. Dachwald, C. Haefßner, Y. Saih, E. Abou-Hamad, I. Llorens, J.-L. Hazemann, K. Köhler, V. D'Elia and J.-M. Basset, *ACS Catal.*, 2016, **6**, 5908–5921.
- B. Beck, M. Harth, N. G. Hamilton, C. Carrero, J. J. Uhrlich, A. Trunschke, S. Shaikhutdinov, H. Schubert, H.-J. Freund, R. Schlögl, J. Sauer and R. Schomäcker, *J. Catal.*, 2012, **296**, 120–131.
- C. A. Carrero, R. Schloegl, I. E. Wachs and R. Schomaecker, *ACS Catal.*, 2014, **4**, 3357–3380.
- K. Chen, A. T. Bell and E. Iglesia, *J. Catal.*, 2002, **209**, 35–42.
- F. Cavani, N. Ballarini and A. Cericola, *Catal. Today*, 2007, **127**, 113–131.
- P. Hu, W.-Z. Lang, X. Yan, L.-F. Chu and Y.-J. Guo, *J. Catal.*, 2018, **358**, 108–117.
- T. Wu, G. Liu, L. Zeng, G. Sun, S. Chen, R. Mu, S. Agbotse Gbonfoun, Z.-J. Zhao and J. Gong, *AIChE J.*, 2017, **63**, 4911–4919.
- P. Bai, Z. Ma, T. Li, Y. Tian, Z. Zhang, Z. Zhong, W. Xing, P. Wu, X. Liu and Z. Yan, *ACS Appl. Mater. Interfaces*, 2016, **8**, 25979–25990.
- S. Sokolov, V. Y. Bychkov, M. Stoyanova, U. Rodemerck, U. Bentrup, D. Linke, Y. P. Tyulenin, V. N. Korchak and E. V. Kondratenko, *ChemCatChem*, 2015, **7**, 1691–1700.
- Y.-P. Tian, P. Bai, S.-M. Liu, X.-M. Liu and Z.-F. Yan, *Fuel Process. Technol.*, 2016, **151**, 31–39.
- G. Liu, Z.-J. Zhao, T. Wu, L. Zeng and J. Gong, *ACS Catal.*, 2016, **6**, 5207–5214.
- U. Rodemerck, S. Sokolov, M. Stoyanova, U. Bentrup, D. Linke and E. V. Kondratenko, *J. Catal.*, 2016, **338**, 174–183.
- U. Rodemerck, M. Stoyanova, E. V. Kondratenko and D. Linke, *J. Catal.*, 2017, **352**, 256–263.
- M. E. Harlin, V. M. Niemi and A. O. I. Krause, *J. Catal.*, 2000, **195**, 67–78.
- S. Sokolov, M. Stoyanova, U. Rodemerck, D. Linke and E. V. Kondratenko, *Catal. Sci. Technol.*, 2014, **4**, 1323–1332.
- M. Ahmadi, H. Mistry and B. Roldan Cuenya, *J. Phys. Chem. Lett.*, 2016, **7**, 3519–3533.
- S. Hanukovich, A. Dang and P. Christopher, *ACS Catal.*, 2019, **9**, 3537–3550.
- S. L. Nauert, L. Savereide and J. M. Notestein, *ACS Catal.*, 2018, **8**, 7598–7607.
- D. E. Keller, S. M. K. Airaksinen, A. O. Krause, B. M. Weckhuysen and D. C. Koningsberger, *J. Am. Chem. Soc.*, 2007, **129**, 3189–3197.
- M. V. Ganduglia-Pirovano, C. Popa, J. Sauer, H. Abbott, A. Uhl, M. Baron, D. Stacchiola, O. Bondarchuk, S. Shaikhutdinov and H. J. Freund, *J. Am. Chem. Soc.*, 2010, **132**, 2345–2349.
- Y. Li, Z. Wei, F. Gao, L. Kovarik, R. A. L. Baylon, C. H. F. Peden and Y. Wang, *ACS Catal.*, 2015, **5**, 3006–3012.
- T. Kropp, J. Paier and J. Sauer, *J. Am. Chem. Soc.*, 2014, **136**, 14616–14625.
- A. Khodakov, J. Yang, S. Su, E. Iglesia and A. T. Bell, *J. Catal.*, 1998, **177**, 343–351.
- C. L. Pieck, M. A. Bañares and J. L. G. Fierro, *J. Catal.*, 2004, **224**, 1–7.
- A. Adamski, Z. Sojka, K. Dyrek, M. Che, G. Wendt and S. Albrecht, *Langmuir*, 1999, **15**, 5733–5741.
- T. P. Otroshchenko, V. A. Kondratenko, U. Rodemerck, D. Linke and E. V. Kondratenko, *Catal. Sci. Technol.*, 2017, **7**, 4499–4510.
- I. E. Wachs, *Dalton Trans.*, 2013, **42**, 11762–11769.
- I. E. Wachs and B. M. Weckhuysen, *Appl. Catal., A*, 1997, **157**, 67–90.
- A. Christodoulakis, *J. Catal.*, 2004, **222**, 293–306.
- Z. J. Zhao, T. Wu, C. Xiong, G. Sun, R. Mu, L. Zeng and J. Gong, *Angew. Chem., Int. Ed.*, 2018, **57**, 6791–6795.
- K. C. Szeto, Z. R. Jones, N. Merle, C. Rios, A. Gallo, F. Le Quemener, L. Delevoeye, R. M. Gauvin, S. L. Scott and M. Taoufik, *ACS Catal.*, 2018, **8**, 7566–7577.
- T. Otroshchenko, S. Sokolov, M. Stoyanova, V. A. Kondratenko, U. Rodemerck, D. Linke and E. V. Kondratenko, *Angew. Chem., Int. Ed.*, 2015, **54**, 15880–15883.
- Y. Zhang, Y. Zhao, T. Otroshchenko, H. Lund, M. M. Pohl, U. Rodemerck, D. Linke, H. Jiao, G. Jiang and E. V. Kondratenko, *Nat. Commun.*, 2018, **9**, 3794.
- Y. Zhang, Y. Zhao, T. Otroshchenko, S. Han, H. Lund, U. Rodemerck, D. Linke, H. Jiao, G. Jiang and E. V. Kondratenko, *J. Catal.*, 2019, **371**, 313–324.
- N. Jeon, H. Choe, B. Jeong and Y. Yun, *Catal. Today*, 2019, DOI: 10.1016/j.cattod.2019.12.012.
- T. Otroshchenko, O. Bulavchenko, H. V. Thanh, J. Rabeah, U. Bentrup, A. Matvienko, U. Rodemerck, B. Paul, R. Kraehnert, D. Linke and E. V. Kondratenko, *Appl. Catal., A*, 2019, **585**, 117189.
- Z. Xie, Y. Ren, J. Li, Z. Zhao, X. Fan, B. Liu, W. Song, L. Kong, X. Xiao, J. Liu and G. Jiang, *J. Catal.*, 2019, **372**, 206–216.
- C. Copéret, A. Comas-Vives, M. P. Conley, D. P. Estes, A. Fedorov, V. Mougel, H. Nagae, F. Núñez-Zarur and P. A. Zhizhko, *Chem. Rev.*, 2016, **116**, 323–421.
- M. K. Samantaray, V. D'Elia, E. Pump, L. Falivene, M. Harb, S. Ould Chikh, L. Cavallo and J.-M. Basset, *Chem. Rev.*, 2020, **120**, 734–813.
- M. K. Samantaray, E. Pump, A. Bendjeriou-Sedjerari, V. D'Elia, J. D. A. Pelletier, M. Guidotti, R. Psaro and J.-M. Basset, *Chem. Soc. Rev.*, 2018, **47**, 8403–8437.



- 44 M. E. Harlin, V. M. Niemi, A. O. I. Krause and B. M. Weckhuysen, *J. Catal.*, 2001, **203**, 242–252.
- 45 J. M. Kanervo, M. E. Harlin, A. O. I. Krause and M. A. Bañares, *Catal. Today*, 2003, **78**, 171–180.
- 46 T. P. Otroshchenko, U. Rodemerck, D. Linke and E. V. Kondratenko, *J. Catal.*, 2017, **356**, 197–205.
- 47 X. Gao, M. A. Bañares and I. E. Wachs, *J. Catal.*, 1999, **188**, 325–331.
- 48 Y.-P. Tian, Y.-A. Liu, X.-M. Liu and Z.-F. Yan, *Catal. Sci. Technol.*, 2018, **8**, 5473–5481.
- 49 Z. Wu, H. S. Kim, P. C. Stair, S. Rugmini and S. D. Jackson, *J. Phys. Chem. B*, 2005, **109**, 2793–2800.
- 50 J. L. Male, H. G. Niessen, A. T. Bell and T. Don Tilley, *J. Catal.*, 2000, **194**, 431–444.
- 51 S. C. Su and A. T. Bell, *J. Phys. Chem. B*, 1998, **102**, 7000–7007.
- 52 I. E. Wachs, *Catal. Today*, 2005, **100**, 79–94.
- 53 C. Zhao and I. E. Wachs, *J. Catal.*, 2008, **257**, 181–189.
- 54 U. Das, G. Zhang, B. Hu, A. S. Hock, P. C. Redfern, J. T. Miller and L. A. Curtiss, *ACS Catal.*, 2015, **5**, 7177–7185.
- 55 C. Xiong, S. Chen, P. Yang, S. Zha, Z.-J. Zhao and J. Gong, *ACS Catal.*, 2019, **9**, 5816–5827.

